HHS Public Access

Author manuscript

Nat Neurosci. Author manuscript; available in PMC 2016 March 01.

Published in final edited form as:

Nat Neurosci. 2015 September ; 18(9): 1325–1333. doi:10.1038/nn.4070.

Identification of Neurodegenerative Factors Using Translatome-Regulatory Network Analysis

Lars Brichta[1], **William Shin**[2,3], **Vernice Jackson-Lewis**[4], **Javier Blesa**[4], **Ee-Lynn Yap**[1], **Zachary Walker**[1], **Jack Zhang**[1], **Jean-Pierre Roussarie**[1], **Mariano J. Alvarez**[2], **Andrea Califano**[2,5], **Serge Przedborski**[4,5], and **Paul Greengard**[1]

[1]Laboratory of Molecular and Cellular Neuroscience, The Rockefeller University, New York, NY 10065, USA

[2]Department of Systems Biology, Columbia University, New York, NY 10032, USA

[3]Department of Biological Sciences, Columbia University, New York, NY 10032, USA

[4]Department of Neurology, Department of Pathology and Cell Biology, and the Center for Motor Neuron Biology and Disease, Columbia University, New York, NY 10032, USA

Abstract

For degenerative disorders of the central nervous system, the major obstacle to therapeutic advancement has been the challenge of identifying the key molecular mechanisms underlying neuronal loss. We developed a combinatorial approach including translational profiling and brain regulatory network analysis to search for key determinants of neuronal survival or death. Following the generation of transgenic mice for cell type-specific profiling of midbrain dopaminergic neurons, we established and compared translatome libraries reflecting the molecular signature of these cells at baseline or under degenerative stress. Analysis of these libraries by interrogating a context-specific brain regulatory network led to the identification of a repertoire of intrinsic upstream regulators that drive the dopaminergic stress response. The altered activity of these regulators was not associated with changes in their expression levels. This strategy can be

Correspondence: Paul Greengard (greengard@rockefeller.edu), Lars Brichta (lbrichta@rockefeller.edu).

[5]Co-senior author

Author Contributions: L.B., M.J.A., A.C., S.P. and P.G. designed experiments; L.B., E.L.Y. and Z.W. generated and characterized Dat bacTRAP mice and performed immunostaining; W.S. created the regulatory model under A.C.'s supervision and carried out the interrogation, leading to the identification of the 19 reported MR genes; L.B. carried out TRAPseq analyses and stereotaxic injections; V.J.L. and J.B. were responsible for MPTP experiments, tissue dissection and stereology; L.B., J.Z., and J.P.R. analyzed expression data. L.B., W.S., M.J.A., A.C., S.P. and P.G. wrote the manuscript.

A supplementary methods checklist is available.

Accession Numbers: Expression data resulting from the reported experiments is available from the Gene Expression Omnibus under accession numbers GSE54795, GSE64452 and GSE64526.

GSE64452 :

Reviewer Access Link : http://www.ncbi.nlm.nih.gov/geo/query/acc.cgi?token=gjijcgoardmfbil&acc=GSE64452

GSE64526 :

Reviewer Access Link : http://www.ncbi.nlm.nih.gov/geo/query/acc.cgi?token=izqvaseijroldmt&acc=GSE64526

GSE54795 :

Reviewer Access Link :http://www.ncbi.nlm.nih.gov/geo/query/acc.cgi?token=wnizumuaxnajhoh&acc=GSE54795

generalized for the elucidation of novel molecular determinants involved in the degeneration of other classes of neurons.

Introduction

Neurodegenerative diseases are debilitating disorders of the central nervous system (CNS) characterized by the progressive loss of distinct neuronal cell populations. Numerous questions exist regarding the molecular mechanisms underlying neuronal degeneration, and the identification of these pathways has proven challenging. As such, effective treatments are scarce. Discovery of the intrinsic factors that determine the survival of neurons and mediate their degeneration would have far-reaching implications for the development of neuroprotective strategies and the therapeutic management of these disorders.

Gene expression profiling is now routinely used to study the phenotypic changes in neurons resulting from pathological events. However, the cellular heterogeneity of the mammalian CNS significantly limits the usefulness of whole tissue for the generation of gene expression profiles specific to the neurons susceptible to degeneration. Investigations based on laser-captured neurons can be cell type-specific, but they rely on the extraction of total cellular RNAs and are not limited specifically to the mRNAs that are translated into proteins. Molecular profiling of distinct cell populations *in vivo* has recently been described using translating ribosome affinity purification (TRAP) [1-3]. However, the application of this methodology to the molecular characterization of vulnerable neurons in the context of various neurodegenerative diseases has been hampered by the limited availability of suitable transgenic TRAP mouse lines. Moreover, TRAP does not improve the downstream analysis and interpretation of gene expression data. Comparing the molecular signatures of cells across various experimental conditions typically identifies a large number of genes whose transcript levels differ significantly. Despite the availability of several bioinformatic tools for the functional analysis of large expression datasets such as the Kyoto Encyclopedia of Genes and Genomes (KEGG) and the Database for Annotation, Visualization and Integrated Discovery (DAVID)[4-6], the prioritization of promising differentially expressed candidate genes has unfortunately remained difficult. Additionally, conventional analyses do not facilitate the identification of the upstream regulators that induce the gene expression changes associated with a pathological phenotype. These shortcomings further hinder the discovery of novel key molecular markers associated with neuronal degeneration.

Using Parkinson's disease (PD) as an example, we developed a strategy for the identification of genes that mediate the response of mature neurons to degenerative insult. The motor manifestations associated with PD are primarily linked to the progressive loss of midbrain dopaminergic (DA) neurons in the substantia nigra pars compacta (SNpc). Therefore, we engineered TRAP transgenic mice that enable the easy, cell type-specific molecular profiling of DA neurons in the midbrain. Using these mice under experimental conditions resembling PD, we generated translational libraries reflecting the molecular signature of the DA neurons at an early stage of degeneration. For the characterization of these libraries, we applied a systems biology approach going beyond differential gene expression analysis. This approach included the accurate assembly and interrogation of a mouse brain regulatory

network, which comprises a comprehensive repertoire of molecular interactions between transcriptional regulators and their target genes. Our analysis revealed a set of intrinsic upstream regulators that mediate the transcriptional response of midbrain DA neurons to a toxic insult triggering degeneration. To validate our data, we applied both expression and functional analyses using a virus-mediated knockdown strategy in DA neurons *in vivo*. We identified transcriptional regulators that are highly and specifically expressed in unperturbed SNpc DA neurons. The loss of these regulators is associated with DA neuron degeneration. Our approach can be applied to other neurodegenerative disorders to discover novel molecular targets for therapeutic intervention.

Results

Generation of TRAP mice for DA neuron profiling

Similar to other types of neurons in the CNS, DA neurons in the midbrain are intermixed with various neuronal and non-neuronal cells. To optimize the cell type-specific molecular profiling of DA neurons, we developed a strategy based on TRAP[1,2]. For this purpose, we generated bacterial artificial chromosome (BAC) transgenic mice in which the expression of enhanced green fluorescent protein (EGFP)-tagged ribosomal protein L10a is controlled by the *dopamine transporter* (*Dat, Slc6a3*) locus. Immunostaining revealed co-localization of the signals for EGFP and the DA neuron marker tyrosine hydroxylase (TH) in all DA neurons at the level of the SNpc and the ventral tegmental area (VTA) without detecting EGFP in non-DA cells (Fig. 1a, b), demonstrating the successful targeted expression of EGFP-L10a specifically in midbrain DA neurons. The EGFP signal was limited to the DA cell bodies and did not expand to the projections of these neurons. This finding indicated that EGFP-tagged ribosomes are either absent from DA projections to the striatum or their number is undetectably low. A signal for EGFP was also obtained in the tuberoinfundibular DA (TIDA) neurons and in the periglomerular DA neurons in the olfactory bulb, suggesting the expression of EGFP-L10a. This finding was expected because these neurons naturally express DAT. However, TIDA and periglomerular DA neurons are located in sufficient anatomical distance to the midbrain DA neurons, allowing for the quick and convenient separation of these neurons from the midbrain before translational profiling.

To demonstrate that Dat bacTRAP mice facilitate the enrichment of translated mRNAs specifically expressed by DA neurons, we dissected the midbrain from Dat bacTRAP mice and affinity-purified translated mRNAs by incubating the tissue lysates with anti-EGFP antibody-coated magnetic beads. From another set of Dat bacTRAP mice, total RNA was extracted from whole midbrain. These samples would be expected to contain RNA from the DA neurons as well as from all intermixed non-DA cell types. Comparative gene expression analysis revealed the significant ($P<0.05$) enrichment of 4382 transcripts in the DA neuron translated mRNA samples as compared to the whole midbrain total RNA samples by ≥1.5fold (Fig. 1c and Supplementary Table 1). As anticipated, all examined DA neuron-specific markers were enriched in the TRAP samples, including *Th* (38fold), *Dat* (*Slc6a3*; 18fold), *vesicular monoamine transporter 2 (Vmat2*, *Slc18a2*; 6fold), *dopamine receptor D2* (*Drd2*; 21fold) and *pituitary homeobox 3* (*Pitx3*; 87fold). In contrast, transcripts that are typically expressed by non-DA cells were enriched ($P<0.05$) in the whole midbrain total

RNA samples and depleted from the DA neuron TRAP samples (Fig. 1c and Supplementary Table 2), including the astrocyte markers *glial fibrillary acidic protein* (*Gfap*; –13fold) and *aldehyde dehydrogenase 1l1* (*Aldh1l1*; –9fold), the gamma-aminobutyric acid (GABA)-ergic neuron marker *vesicular GABA transporter* (*Vgat*, *Slc32a1*; –4fold), the glutamatergic neuron marker *vesicular glutamate transporter 1* (*Slc17a7*; –11fold), and the endothelial cell marker *thrombomodulin* (*Thbd*; –27fold). The clear enrichment of DA neuron markers in the TRAP samples and the depletion of non-DA transcripts suggested that Dat bacTRAP mice are suitable for the cell type-specific translational profiling of midbrain DA neurons.

Characterization of Dat bacTRAP mice

Dat bacTRAP mice present normal brain morphology (Supplementary Fig. 1a). Transgenic (TG) animals are lighter than wildtype (WT) littermates, but do not differ in their key parameters of body composition, food or water intake (Supplementary Fig. 1b–e). Hemizygous Dat bacTRAP mice carry a stable tandem insert of 6–10 BAC transgenes on chromosome 9q (Supplementary Fig. 2). Importantly, we did not observe any morphological differences in the general structure of the DA system or the shape of single DA neurons between TG Dat bacTRAP mice and WT littermates (Supplementary Fig. 3a). Additional analyses revealed similar numbers of TH-positive (TH^+) neurons in the SNpc and in the VTA, similar striatal levels of dopamine and its metabolites, and comparable striatal levels of TH and DAT in adult TG Dat bacTRAP mice and their WT littermates (Supplementary Fig. 3b–e). Taken together, these data indicated that the expression of the EGFP-L10a transgene did not lead to any measureable alterations of the morphological, stereological or biochemical characteristics of the midbrain DA neurons in Dat bacTRAP mice.

Additionally, we examined the performance of Dat bacTRAP mice in behavioral paradigms that assessed coordination, muscle strength and gait. Data obtained for the rotarod test, the pole test and the wire hang test did not demonstrate any differences between TG Dat bacTRAP mice and their WT littermates (Supplementary Fig. 4). Analysis of the foot print patterns at three months of age revealed comparable gait parameters for TG and WT mice (Supplementary Fig. 5a). Older TG Dat bacTRAP mice demonstrated a small but significant reduction of their hindlimb width and forelimb/hindlimb overlap compared to WT littermates (Supplementary Fig. 5b–d). Although a greater forelimb/hindlimb overlap signals motor impairment[7], the reduction of forelimb/hindlimb overlap or hindlimb width is not associated with pathological changes and may be due to the increasing weight difference between aging WT and TG mice in our study (Supplementary Fig. 1b).

Translational profiling of DA neurons in a model of PD

After demonstrating the utility of Dat bacTRAP mice for the isolation of translated mRNAs from midbrain DA neurons, we were next interested in the application of our methodology to the molecular profiling of midbrain DA neurons in a model of PD. It seemed reasonable that this approach would deliver cell type-specific gene expression data reflecting intrinsic pathological changes in DA neurons under experimental conditions resembling key features of the disease in humans. For this purpose, we decided to use the MPTP-induced mouse model. MPTP is a toxin that specifically targets DA neurons in both humans and mice and reproduces the degeneration of SNpc DA neurons associated with PD[8]. The MPTP mouse

model is extremely well established, and widely considered the most suitable available mouse model to investigate the molecular mechanisms that are involved in DA neuron degeneration[9,10].

To validate the potency of MPTP in Dat bacTRAP mice, one group of TG animals and WT littermates were injected with either saline (vehicle) or MPTP following a subacute dosing regimen. Consistent with published data[11], MPTP reduced the number of SNpc TH^+ neurons in this group of Dat bacTRAP mice to ∼53% by 21 days after final injection, which reflects the time point at which the DA neuron lesion is stable (Supplementary Fig. 6). No difference was observed between WT and TG animals. In the same group of mice, we also investigated the impact of the subacute MPTP regimen on the number of DA neurons in the VTA. Although SNpc and VTA DA neurons produce the same neurotransmitter and are localized in close proximity to each other in the midbrain, VTA DA neurons are less susceptible to degeneration in patients with PD[12,13]. The differential vulnerability of SNpc and VTA DA neurons was successfully reproduced in mice injected with MPTP[14,15]. In agreement with these studies, we found that the subacute dosing schedule of MPTP reduced the number of VTA TH^+ neurons in Dat bacTRAP mice only to ∼71% by 21 days after the final injection (Supplementary Fig. 6). These data indicated that the differential vulnerability of SNpc and VTA DA neurons is maintained in Dat bacTRAP mice.

To carry out cell type-specific translational profiling of midbrain DA neurons, a second group of Dat bacTRAP mice was injected with saline (vehicle) or MPTP following the subacute dosing regimen. In contrast to the experimental concept used for the validation of MPTP potency, Dat bacTRAP mice designated for translational profiling and expression analysis by RNA sequencing (TRAPseq) were sacrificed four days after the last MPTP injection (Fig. 2a). At this time point, the number of SNpc DA neurons that are still viable but poised to die is maximal[11]. We reasoned that this strategy would allow us to profile SNpc DA neurons under stress at a very early stage of degeneration rather than carrying out translational profiling at a stage mimicking advanced PD. Compared to animals injected with saline (vehicle), expression of the DA neuron phenotypic marker *Th* was moderately reduced to 73±4% (mean±SEM; normalized to β-actin; P=0.030, unpaired t-test) in MPTP-treated Dat bacTRAP mice four days after the last injection, validating that the DA neurons in these animals were under toxin-induced stress[16]. Analysis of the cell type-specific translatome libraries reflecting the molecular profiles either of unperturbed midbrain DA neurons in saline-treated Dat bacTRAP mice or of DA neurons under toxin-induced stress in MPTP-treated Dat bacTRAP mice revealed a number of genes with significantly different expression between the two groups (Fig. 2b and Supplementary Table 3).

Identification of upstream regulators of neurodegeneration

Numerous attempts to elucidate the molecular determinants underlying progressive cell loss in neurodegenerative disorders have exclusively relied on the comparison of gene expression levels in normal and pathological tissue. Unfortunately, this approach typically does not go beyond the generation of comprehensive lists of differentially expressed genes which are ranked based on the fold change of their transcript levels. In particular, the discovery of key upstream regulators that cause the observed gene expression changes is not supported by this

analysis. An innovative systems biology approach to identify molecular targets for disease therapy has recently been described in the field of cancer research[17-20]. In a first step, a tissue-specific network that maps relationships between downstream target genes and their upstream transcriptional regulators was computationally generated using the ARACNe algorithm[21]. This step was followed by the interrogation of the engineered network with genome-wide expression signatures obtained from control and cancer tissues: for each transcriptional regulator included in the network, the mapped downstream target genes were tested for differential expression in cancer tissue. Thus, each set of downstream target genes represents a comprehensive gene reporter assay for activity changes of the corresponding upstream transcriptional regulator. Transcriptional regulators that drive the gene expression signature in cancer tissue were identified by the significant enrichment of differentially expressed, mapped target genes. These regulators are termed Master Regulators (MRs), and the analysis is referred to as MAster Regulator INference Algorithm (MARINa).

The basic principles of MARINa are not limited to the investigation of particular tumor types, and have also shown promise for the discovery of disease determinants in non-cancerous conditions[22-24]. Thus, we hypothesized that the application of this methodology to the analysis of our cell type-specific DA neuron translatome libraries would facilitate the discovery of novel genes that determine DA neurodegeneration. We reverse engineered a regulatory network from a mouse whole brain expression dataset consisting of 437 tissue samples (GSE10415) using ARACNe. The resulting adult mouse brain regulatory network contained 338,550 interactions between 1,345 transcriptional regulators and 16,527 target genes. Next, using the genome-wide translatome signatures we had obtained for unperturbed midbrain DA neurons in saline-treated Dat bacTRAP mice or for DA neurons in MPTP-treated Dat bacTRAP mice, we interrogated the mouse whole brain regulatory network to identify key transcriptional regulatory proteins that mediate the response of DA neurons to degenerative stress. MARINa analysis identified 19 MR candidates that drive the molecular signature of midbrain DA neurons at a very early stage of degeneration (Fig. 2c and Supplementary Table 4). Ten MRs aberrantly increased their regulatory activity after the challenge with MPTP. The remaining nine MRs decreased their activity.

We then investigated the translated mRNA levels of the 19 identified MR candidates in DA neuron TRAP samples from mice that received either saline (vehicle) or MPTP. This analysis revealed that the changes in MR transcriptional activity between saline and MPTP samples (Fig. 2c) were not associated with differential MR gene expression (Fig. 2d), raising the possibility that post-translational regulation of the MRs is responsible for their altered transcriptional activities. Our findings are consistent with the results obtained in several cancer phenotypes[17,19,20] and show that these MRs could not have been identified by conventional means relying exclusively on the examination of fold differences in transcript levels.

Subtype-specific profiling of SNpc and VTA DA neurons

Discovery of the 19 MR candidates (Fig. 2c) was based on the analysis of TRAP data obtained from both SNpc and VTA DA neurons. SNpc DA neurons are more vulnerable to degeneration in PD than VTA DA neurons. Therefore, to gain insight into the molecular

alterations that are specific to the response of SNpc DA neurons to degenerative stress, we were especially interested in identifying MR candidates with higher baseline gene expression levels in SNpc DA neurons which may point to a specific physiological relevance of these MRs for the SNpc. To compare the baseline expression levels of the 19 MR candidates in SNpc and VTA DA neurons, we dissected and separated the SNpc and VTA from Dat bacTRAP mice and carried out TRAPseq. Comparative analysis of the translatome libraries confirmed the significantly higher expression of previously reported markers in SNpc DA neurons, including *aldehyde dehydrogenase 1a7* (*Aldh1a7*, 4.7fold), *Cd24a antigen* (3.1fold) and *thyrotropin-releasing hormone receptor* (*Trhr*, 2.6fold) (Supplementary Fig. 7a and Supplementary Table 5)[25]. We also confirmed the significantly higher levels of previously published transcripts in VTA DA neurons, such as *lipoprotein lipase* (*Lpl*, 4.5fold), *orthodenticle homolog 2* (Otx2, 4.2fold) and *gastrin releasing peptide* (*Grp*, 3.5fold) (Supplementary Fig. 7a and Supplementary Table 6)[25]. These data demonstrated the successful dissection of SNpc and VTA from Dat bacTRAP mice as well as the purification of DA neuron subtype-specific translated mRNAs. We then compared the transcript levels of the 19 MR candidates in our SNpc and VTA DA neuron TRAP samples (Fig. 3a). This analysis revealed that two of the MR candidates were more highly expressed in SNpc DA neurons than in VTA DA neurons, including *DNA-binding protein Satb1* (*Satb1*, 1.6fold) and *palmitoyltransferase Zdhhc2* (*Zdhhc2*, 1.8fold). A survey of the expression patterns of *Satb1* and *Zdhhc2* using the Allen Mouse Brain Atlas (http://mouse.brain-map.org) confirmed that *Satb1* and *Zdhhc2* mRNAs, as visualized by *in situ* hybridization, are highly abundant in the SNpc in ventral midbrain (Supplementary Fig. 7b–d).

Next, to validate the higher expression of *Satb1* and *Zdhhc2* in SNpc DA neurons, we investigated the anatomical distribution of SATB1 and ZDHHC2 protein in the midbrain. The signal for SATB1 co-localized with that for TH, which is consistent with a previous immunohistochemistry study[26] and suggested that SATB1 is specifically expressed in DA neurons (Fig. 3b). Importantly, SATB1 was indeed expressed at higher levels in the SNpc compared to the VTA (Fig. 3b), and its expression was confined to the nucleus of DA neurons (Fig. 3c). For ZDHHC2, we also observed higher expression in the SNpc compared to the VTA (Fig. 3d). In the DA neurons, the immunoreactivity for ZDHHC2 and the Golgi marker GM130 partially overlapped, pointing to a localization of ZDHHC2 in the Golgi apparatus (Fig. 3e). However, part of the ZDHHC2 signal did not co-localize with that for TH, suggesting that ZDHHC2 is not confined exclusively to the DA neurons (Fig. 3e).

In summary, our results led us to conclude that unperturbed SNpc DA neurons in particular are characterized by the high expression of SATB1 and ZDHHC2. Together with the findings from our regulatory network analysis, which suggested that the regulatory activities of SATB1 and ZDHHC2 are reduced in DA neurons at an early stage of degeneration, we reasoned that SATB1 and ZDHHC2 may represent intrinsic DA neuron pro-survival factors whose loss of function is associated with DA cell death.

Importantly, congruent with *Satb1* and *Zdhhc2* mRNA quantification in mice that received either saline or MPTP (Fig. 2d), Western blot analysis demonstrated that the altered transcriptional activities of SATB1 and ZDHHC2 four days after MPTP treatment (Fig. 2c)

were not associated with changes in the protein levels of these two MRs (Supplementary Fig. 7e, f and Fig. 3f, g). This further validated that SATB1 and ZDHHC2 could not have been identified using conventional expression analyses and that the MR activity changes may be due to the post-translational regulation of these proteins in the DA neurons.

Validation of novel determinants of DA neurodegeneration

A recent investigation in developing cortical interneurons in mice reported that the knockout of SATB1 interferes with the migration, differentiation, connectivity and survival of these cells[27]. These findings supported our results which indicated that SATB1 represents a pro-survival factor in mature DA neurons. However, to validate the role of SATB1 and ZDHHC2 in SNpc DA neurons, and to demonstrate that our methodology consisting of translatome and regulatory network analysis is a powerful approach for the identification of key determinants involved in neuronal degeneration, we investigated the consequences of SATB1 or ZDHHC2 knockdown on the survival of DA neurons. In one group of adult WT mice, each animal was stereotaxically injected with a *Satb1* shRNA-EGFP construct into the left SNpc and a scrambled shRNA-EGFP control vector into the right SNpc (Fig. 4a). Knockdown of SATB1 mimicked the effect of MPTP, causing a 79.5±6.8% (mean±SEM; n=6 biological replicates; P=0.0004, paired t-test) reduction in the number of SNpc TH^+ neurons as compared to the control SNpc eight weeks after viral injection. The number of $Nissl^+$,TH^- neurons remained unaffected (Supplementary Fig. 8a). These results were verified with a second *Satb1* shRNA (Supplementary Fig. 8b, c). SNpc TH^+ neurons disappeared in two stages. First, by two weeks after viral injection of the *Satb1* shRNA-EGFP vector, SATB1 was already undetectable, rendering SNpc DA neurons dysfunctional as demonstrated by the substantially reduced immunoreactivity of SNpc $EGFP^+$ neurons for the phenotypic marker TH (Fig. 4b, c). Second, at three (Fig. 4d) and four (Supplementary Fig. 8d) weeks after stereotaxic surgery, very few $EGFP^+$ or TH^+ cells were detected in the SNpc, suggesting the loss of SNpc DA neurons. Furthermore, we stereotaxically injected mice with Fluorogold (FG) into the left and right dorsal striatum to retrogradely label SNpc DA neurons. The same animals were then injected with viral shRNA vectors according to Fig. 4a. SNpc DA neurons labeled with FG also disappeared after *Satb1* silencing (Supplementary Fig. 8e). We thus concluded that the decreased number of SNpc TH^+ cells after SATB1 knockdown reflects true cell loss and not merely loss of TH expression. To provide biochemical evidence that the target genes identified by ARACNE (Fig. 2c and Supplementary Table 4) are indeed regulated by the respective MR, we injected Dat bacTRAP mice according to Figure 4a and analyzed knockdown and control samples by TRAPseq early in the course of DA neurodegeneration. *Satb1* mRNA levels in knockdown samples were reduced to 33±10% (mean±SEM, n=3 biological replicates, P=0.0170, paired t-test) compared to controls. Using Gene Set Enrichment Analysis (GSEA), ARACNE-identified SATB1 target genes were ranked according to their differential expression between knockdown and control samples. Strikingly, *Satb1* silencing was associated with decreased SATB1 activity (indicated by a negative NES) and the significant enrichment of downregulated SATB1 target genes (Fig. 4e and Supplementary Table 7), recapitulating the results obtained in MPTP-injected mice.

In another group of adult WT mice, each animal was stereotaxically injected with a *Zdhhc2* shRNA-RFP vector into the left SNpc while a scrambled shRNA-EGFP control vector was injected into the right SNpc (Fig. 5a). Similar to the results obtained for SATB1, knockdown of ZDHHC2 led to a 96.6±0.6% (mean±SEM; n=5 biological replicates; P=0.0007, paired t-test) reduction in the number of SNpc TH^+ neurons as compared to the control SNpc eight weeks after viral injection. The number of $Nissl^+$,TH^- neurons was also reduced to 49.5±6% (Supplementary Fig. 8f). This finding suggested that non-DA neurons are affected by the ZDHHC2 knockdown, which may be related to the observation of a signal for ZDHHC2 in the unperturbed SNpc that did not co-localize with TH (Fig. 3e). Using a second *Zdhhc2* shRNA, a similar trend was observed, although the results were not statistically significant (Supplementary Fig. 8g, h). SNpc TH^+ neurons also disappeared in two stages after ZDHHC2 knockdown. First, by one week after injection of the *Zdhhc2* shRNA-RFP vector, ZDHHC2 was already undetectable which negatively impacted the function of SNpc DA neurons as suggested by the diminished immunoreactivity of SNpc RFP^+ neurons for TH (Fig. 5b, c). Second, at two (Fig. 5d) and three (Supplementary Fig. 8i) weeks after viral injection, neither RFP^+ nor TH^+ cells were detected in the SNpc, suggesting the loss of SNpc DA neurons. Stereotaxic injection of mice with FG into the left and right dorsal striatum followed by intranigral injection of viral shRNA vectors according to Fig. 5a showed that SNpc DA neurons labeled with FG disappeared after *Zdhhc2* silencing (Supplementary Fig. 8j). This observation resembled our findings obtained after SATB1 knockdown and suggested that the decreased number of SNpc TH^+ cells after ZDHHC2 knockdown also reflects true loss of cells and not merely the abolished expression of the phenotypic marker TH.

To further validate our findings, we investigated if SATB1 and ZDHHC2 can be identified as MRs of human DA neuron pathology at an early stage of PD that is comparable to the time point we chose for the TRAPseq analysis in the MPTP mouse model (Fig. 2a). Therefore, we carried out a regulatory network analysis on expression profiles obtained from SN samples from incipient PD cases and controls[28]. Strikingly, this analysis confirmed the significantly decreased transcriptional activities of SATB1 and ZDHHC2 in patients with incipient PD (Fig. 6). Consistent with our data obtained in mice, these changes were not associated with changes in the expression levels of *SATB1* and *ZDHHC2* (Fig. 6).

Discussion

Cell type-specific translational profiling of distinct groups of degenerating neurons in combination with the analysis of a context-specific regulatory network is a novel approach to identify intrinsic molecular factors that drive neuronal loss. As part of this strategy, the generation and application of suitable TRAP mouse lines enables the comprehensive analysis of neurons at any desired degenerative stage in animal models of human disorders. Such studies provide the opportunity to discover early molecular markers of the disease process. Similarly, the application of a context-specific regulatory network for the analysis of neuronal gene expression signatures is not limited to a certain stage of degeneration. The most significant technical advantage provided by regulatory network analysis is the identification of neuron-intrinsic transcriptional regulators that are effectors of the recorded gene expression differences. The characterization of hundreds of differentially expressed

genes one by one is replaced by the discovery of respective upstream regulators of these genes.

Translational profiling of DA neurons

We selected PD as a major neurodegenerative disorder of the CNS and developed a methodology for the characterization of DA neuron degeneration. Dat bacTRAP mice enable the cell type-specific translational profiling of midbrain DA neurons *in vivo*. Previous studies focusing on gene expression profiling of unperturbed midbrain DA neurons in rodents predominantly relied on whole midbrain or laser-captured neurons[25,29,3031-33]. However, the analysis of whole midbrain is not specific to DA neurons, and laser-capture microdissection often results in poor RNA yield and quality. Fluorescence-activated cell sorting (FACS) has been carried out to isolate DA neurons from midbrain tissue from mice expressing EGFP under the control of the *Th* promoter[34]. Unfortunately, FACS most likely confounds the true molecular signature of the DA neurons due to stress during cell isolation and the loss of input signals from neighboring cells and other innervating neurons. In contrast, the use of Dat bacTRAP mice represents a straight-forward methodology enabling efficient, cell type-specific isolation of translated mRNAs from DA neurons *in vivo* without prior fixation, staining, dissociation or sorting of these cells.

Regulatory network analysis and identification of MRs

Investigation of our translatome libraries facilitated the identification of novel MRs of early DA neuron degeneration. The analysis presented an unbiased approach that equally considers the involvement of each of the transcriptional regulators included in the brain regulatory network. Importantly, our combinatorial approach consisting of translatome and regulatory network analysis facilitated the identification of those genes undetectable exclusively by comparing gene expression levels.

The comparative TRAPseq analysis of SNpc and VTA DA neurons provided a useful data resource for translated mRNAs that are enriched in either of the two cell types, which may facilitate the discovery of genes with a role in differential DA neuron vulnerability. Interestingly, eight MR candidates were more highly expressed in VTA DA neurons than in SNpc DA neurons, and several of these regulators increased their activity after the challenge with MPTP. These findings may indicate a connection between the elevated activity of these MRs and the decreased vulnerability of VTA DA neurons to degeneration, warranting further investigation. The group of MRs with similar expression levels in SNpc and VTA DA neurons included myocyte-specific enhancer factor (MEF) 2A and methyl-CpG-binding protein 2 (MECP2), both of which decreased their regulatory activity under MPTP-induced stress. Reduced transcriptional activity of another MEF2 isoform, MEF2C, in a human stem cell-derived DA neuron model of PD was recently reported, while the protein levels of MEF2 did not change[35]. MEF2C plays an important role in DA neurogenesis and differentiation in embryonic stem cells[36,37]. However, in mouse adult SNpc DA neurons *in vivo*, Mef2a expression levels (Fig. 2d) are much higher than those of Mef2c (FPKM<1), suggesting that the two isoforms possibly fulfill similar functions in the two model systems. Studies in mutant MECP2 mice have demonstrated alterations in the survival and function of DA neurons[38,39]. In agreement with a pro-survival function of MECP2 in DA neurons, our

translatome-regulatory network analysis found a decreased activity for MECP2 in degenerating DA neurons, further demonstrating the validity of our methodology.

Validation of novel drivers of SNpc DA degeneration

SATB1 and ZDHHC2 represent two novel endogenous neuroprotective proteins which may have evolved as a protective mechanism for SNpc DA neurons. The enrichment of SATB1 and ZDHHC2 in adult SNpc DA neurons appears to reflect an intrinsic defense mechanism that opposes neurodegeneration. Both proteins are required to maintain the DA phenotype, and the disruption of their function is sufficient to induce DA neuron degeneration. The concept of protective factors being highly expressed in the vulnerable SNpc DA neurons is in contrast to the traditional hypothesis that protective genes are expressed particularly in the more resistant VTA DA neurons. However, it has been demonstrated that SNpc DA neurons are under tonic cellular stress[40-42], which may explain the elevated need for intrinsic protection as compared to VTA DA neurons. Disruption of essential SNpc-specific protective mechanisms is likely to result in rapid cell death. SATB1 is a transcriptional regulator and DNA organizer[43] localized to the nucleus. In contrast, we detected ZDHHC2 in the Golgi apparatus of DA neurons. Based on this observation, it seems unlikely that ZDHHC2 directly regulates the expression of its target genes. However, ZDHHC2 is able to palmitoylate other proteins[44] which can result in the modulation of protein-protein interactions, thereby eventually altering transcription[45]. Although the down-regulation of SATB1 and ZDHHC2 appears to contribute to SNpc DA neuron degeneration, viral overexpression of SATB1 or ZDHHC2 in SNpc DA neurons in mice had no effect on MPTP-induced neurodegeneration (data not shown), suggesting a limited role of these two proteins specifically in the MPTP model of DA neuron toxicity.

In the context of our studies, it would also be of interest to search for candidate modulators of MR activity by applying algorithms such as MINDy[46]. Moreover, the DIGGIT algorithm[22] can facilitate the integration of GWAS data with regulatory transcriptional and post-transcriptional models of cellular control. This approach may be instrumental in elucidating causal genetic determinants predisposing to disease. However, this analysis would not facilitate the identification of the actual target sites of the post-translational modifications that potentially impact the transcriptional activity of SATB1 and ZDHHC2.

The identification and validation of SATB1 and ZDHHC2 clearly demonstrates that our strategy consisting of translational profiling of degenerating neurons and the analysis of a context-specific brain regulatory network can successfully be applied to the discovery of novel determinants of neuronal loss. Importantly, we confirmed the decreased activities of SATB1 and ZDHHC2 in patients with incipient PD. Based on the present investigations, it appears feasible to apply a similar strategy to the characterization of distinct groups of degenerating neurons in models of disorders other than PD, including Alzheimer's disease, spinal muscular atrophy, Huntington's disease and amyotrophic lateral sclerosis.

Methods

Animals

All experiments were approved by the Rockefeller University or Columbia University Institutional Animal Care and Use Committee and were performed in accordance with the guidelines described in the US National Institutes of Health Guide for the Care and Use of Laboratory Animals. Mice were housed in rooms on a 12 h dark/light cycle at 22 °C and maintained with rodent diet (Picolab) and water available *ad libitum*. Male mice were used for all experiments. Mice were housed in small groups of up to five animals, except for mice that underwent stereotaxic surgery which were housed singly to ensure recovery and avoid fighting.

Generation of Dat bacTRAP mice

Dat bacTRAP TG mice were generated on a C57BL/6 (Charles River Laboratories) background according to published protocols[47], with the exception that the EGFP-L10a transgene was used in place of EGFP. BAC RP24-269I17 was used to place the sequence of EGFP-L10a under the control of the mouse *Dat* (*Slc6a3)* locus. Dat bacTRAP mice breed normally and inherit the transgene in a Mendelian manner. Genotyping was carried out by Transnetyx, using a probe and primer set detecting the junction between the sequences of the *Dat* locus and the EGFP-tag. Mice were maintained as hemizygotes.

MPTP injections

All MPTP experiments used the subacute regimen consisting of one daily intraperitoneal injection of MPTP-HCl (30 mg/kg free base per day) for five consecutive days. Control animals received vehicle (saline) injections only. To evaluate MPTP potency in four-month-old male TG Dat bacTRAP mice and WT littermates (Supplementary Fig. 6), animals were killed 21 days after the last injection. For the TRAPseq analysis of midbrain DA neurons (Fig. 2), animals were killed four days after the last injection. MPTP use and safety precautions were as described[9].

TRAPseq and gene expression analysis

To compare Dat bacTRAP translated mRNA samples with whole midbrain total RNA samples, 12 four-month-old Dat bacTRAP mice were randomly divided into four groups of three mice, followed by the dissection of the midbrain from all animals and purification of translated mRNAs as described below. From another five four-month-old Dat bacTRAP mice, total RNA was extracted from whole midbrain using the RNAqueous Total RNA Isolation Kit (Life Technologies). For the TRAP analysis of midbrain DA neurons (SNpc and VTA combined) in a model of PD, 12 four-month-old Dat bacTRAP mice were injected with saline and randomly divided into four groups of three mice, and 12 four-month-old Dat bacTRAP mice were injected with MPTP and randomly divided into four groups of three mice. From each mouse, the whole midbrain was dissected. For the comparative TRAP analysis of SNpc DA neurons and VTA DA neurons, 30 four-month-old Dat bacTRAP mice were randomly divided into six groups of five mice. Brains were removed and sectioned using an ice-cold Adult Mouse Brain Slicer with 1 mm coronal slice intervals (Zivic

Instruments). From the tissue section containing the midbrain, the SNpc and VTA regions were dissected and separated under a Nikon SMZ645 light microscope using a 10× lens. TRAP analysis on stereotaxically injected Dat bacTRAP mice was carried out two weeks after *Satb1* silencing. Mice were divided into three groups of five mice. Brains were removed and the midbrains were dissected, followed by separation of the ipsilateral (*Satb1* shRNA) and contralateral (scrambled shRNA) sides.

Translated mRNAs were purified from bacTRAP mice as described previously[48]. Male hemizygous Dat bacTRAP mice were used for all TRAP analyses. TRAP samples underwent DNase digestion using the RNase-Free DNase Set (Qiagen) and were subsequently purified with the RNeasy MinElute Cleanup Kit (Qiagen). Eluted RNA samples were analyzed on a 2100 Bioanalyzer (Agilent) using RNA Pico Chips (Agilent) to confirm RNA integrity, followed by the measurement of RNA concentrations with the Quant-iT RiboGreen RNA Assay Kit (Life Technologies). cDNAs were prepared with the Ovation RNA-Seq System V2 kit (NuGEN), using an input of either 2.5 ng RNA (TRAP samples from SNpc and VTA DA neurons combined) or 1 ng RNA (TRAP samples from either SNpc DA neurons or VTA DA neurons). 500 ng cDNA from each sample were fragmented on a Covaris S2 Focused Ultrasonicator using the operating conditions recommended by the manufacturer for a target fragment size of 200 bp. Fragment size was confirmed on a 2100 Bioanalyzer using High Sensitivity DNA Chips (Agilent). Libraries for RNA sequencing were prepared with the TruSeq RNA Sample Preparation v2 kit (Illumina), starting the manufacturer's low-throughput protocol with the end repair step. The concentration of the RNA-Seq libraries was determined on a 2100 Bioanalyzer using High Sensitivity DNA Chips. Subsequently, two libraries with different adapters were multiplexed for sequencing. After confirming the concentration of the multiplexed samples on a 2100 Bioanalyzer using High Sensitivity DNA Chips, samples were analyzed on an Illumina HiSeq 2000 sequencer using 100 bp single-end sequencing. To compose MPTP and vehicle translatome libraries, RNA-Seq reads were first mapped to the Mus musculus assembly nine reference genome using Bowtie[49]. Reads mapping to known genes, based on Entrez gene identifiers, were then counted using the GenomicFeatures R-system package (Bioconductor)[50]. Differential expression (Supplementary Table 3) was calculated using DESeq version 1.20.0 and R version 3.1.1. For all other RNA-Seq analyses, reads were mapped to the Mus musculus assembly 10 reference genome using TopHat[51] version 2.0.11. FPKM values for all genes in each sample were calculated with Cufflinks[52] version 2.2.1. To analyze differential gene expression between samples (Supplementary Tables 1, 2, 5 and 6), DESeq[53] version 1.14.0 was used under the standard comparison mode. *P* values were reported by DESeq, adjusted for multiple testing using the Benjamini-Hochberg procedure.

Unbiased stereology

The total number of TH^+ neurons and $Nissl^+$ TH^- neurons was quantified by unbiased stereology using the optical fractionator method as described[54]. This unbiased method of cell counting is not affected by either the volume of reference (SNpc or VTA) or the size of the counted elements (neurons). Animals were perfused with 1 × PB followed by 4 % paraformaldehyde in 1 × PB, the brains were post-fixed in 4 % paraformaldehyde, cryoprotected in 30 % sucrose, frozen and stored at -80 °C until sectioning. 30-μm-thick

free-floating coronal sections were prepared from the midbrain using a cryostat and every fourth section was used for cell counting. For TH immunohistochemistry, sections were incubated with a rabbit polyclonal anti-TH antibody (Calbiochem, #657012) at a concentration of 1:2,000 at 4 °C for 48 h, followed by a biotinylated polyclonal goat anti-rabbit IgG (Vector Laboratories, #BA1000) at 1:400 for 60 min, streptavidin-conjugated horseradish peroxidase for 60 min (Vector Laboratories, #PK-4000) and 3,3′-diaminobenzidine (DAB). Stained sections were mounted onto slides, counterstained with thionin to visualize Nissl substance, and coverslipped.

Measurement of striatal dopamine, 3,4-dihydroxyphenylacetic acid (DOPAC), and homovanillic acid (HVA)

Four-month-old male animals were killed at the 21-days time point and the striata were dissected and processed. The levels of dopamine, DOPAC and HVA were determined by high performance liquid chromatography as described[55], with minor modifications of the mobile phase. The modified mobile phase consisted of 90 % 0.05 M potassium phosphate, 250 mg/l heptane sulphonic acid, 0.1 mM EDTA pH 2.8, and 10 % methanol.

Regulatory networks assembly

The regulatory network was reverse engineered from a phenotypically diverse mouse brain expression dataset obtained from seven brain regions (hippocampus, cerebellum, olfactory bulb, basal ganglia, frontal cortex, cingulate cortex, amygdala) from six- to eight-week-old laboratory mice belonging to 20 different inbred strains (437 samples, GSE10415) using ARACNe[21]. ARACNe was run with 100 bootstrap iterations using all probes that mapped to a set of 1,507 mouse transcriptional regulators which were defined as genes annotated as GO:0003700 - ‘transcription factor activity’ in the Gene Ontology Molecular Function database[56]. Parameters were set to 0 DPI tolerance and a MI *P* value threshold ($P<10^{-7}$), as recommended for bootstrap ARACNe analysis of a dataset with this size, to achieve a Bonferroni corrected significance ($P = 0.05$) for getting a single false-positive in the dataset. The regulatory network used in our study is available for download from figshare (http://dx.doi.org/10.6084/m9.figshare.926507).

MR analyses on mouse translatomes

To define the MPTP-specific genome-wide expression signature for midbrain DA neurons, we composed a list of all genes, arranged from the gene with the most down-regulated expression in response to MPTP to the gene with the most up-regulated expression. Differential expression was computed by comparing MPTP and saline (vehicle) samples using Student's t-test after normalizing the raw counts by a negative binomial-based variance stabilizing transformation (VST) implemented in the DESeq package (Bioconductor). MRs were obtained from the MPTP-specific signature using the MARINa algorithm together with the mouse whole brain regulatory network[18,19]. The MARINa algorithm used in our studies is an improved version of the original algorithm[18,19] with the following modifications: (i) it tests for a global shift in the position of the regulons when projected on the gene expression signature instead of using the Kolmorogov-Smirnov test statistics; (ii) it uses a probabilistic framework to integrate knowledge of activated, repressed, and non-monotonically regulated

transcriptional targets; (iii) it takes into account pleiotropic regulation of each target gene by multiple regulators when computing the enrichment. Statistical significance, including *P* value and normalized enrichment score (NES), was estimated by comparison to a null model generated by permuting the samples uniformly at random 1,000 times. The MARINa algorithm is implemented in the ssMARINA R-package and available for download from figshare (http://dx.doi.org/10.6084/m9.figshare.785718). The results of the MR analysis have been recorded as a Sweave document, which is designed to outline the set-up and running of MARINa on the saline- and MPTP-specific translatomes. When compiled, the document will run the computational analysis described in the manuscript and present the results as a table and plot (corresponding to Fig. 2c). The Sweave document, associated pdf document, and files needed for the execution of the Sweave file can all be downloaded at the following figshare link: http://dx.doi.org/10.6084/m9.figshare.1279439.

MR analysis on PD expression signatures—Analysis was carried out on a dataset obtained from SN samples from 16 cases with incipient PD and 17 controls (Gene Expression Omnibus accession #GSE20159)[28]. Data was downloaded and converted into Entrez Gene IDs to allow for the comparison with the humanized mouse brain regulatory network. For genes that mapped to multiple probesets, the probeset with the highest coefficient of variation was used. MARINa was run using the predictions of the mouse brain regulatory network converted to homologous human Entrez Gene IDs using a database from the Mouse Genome Informatics (MGI) website (http://www.informatics.jax.org/). Incipient PD samples were compared with control samples by Student's t-test and significance was assessed using 10,000 gene label-shuffling randomizations with the Bonferroni method used for multiple hypothesis correction. The humanized mouse brain regulatory network used in this analysis is available for download from figshare (http://dx.doi.org/10.6084/m9.figshare.942420).

GSEA analysis—Gene Set Enrichment Analysis was performed as described[57] using an in-house implementation in R 3.0.1. Statistical significance was estimated by comparison to a null model generated by permuting the gene labels uniformly at random 10,000 times. The datasets used for GSEA analysis of SATB1 target genes on differentially expressed genes between SATB1 control and SATB1 knockdown TRAP samples are available for download from figshare (http://dx.doi.org/10.6084/m9.figshare.926518).

qRT-PCR

To analyze gene expression levels, cDNA was generated as described above and used as the template for qRT-PCR on a Real-Time Thermal cycler (Life Technologies). Taqman Universal PCR Master Mix, no AmpErase UNG (Life Technologies) was used for all analyses. Taqman gene expression assays (FAM) from Life Technologies were as follows: *Actb* (Mm01205647_g1) and *Th* (Mm00447557_m1).

To determine the number of genomic *Slc6a3* copies, DNA isolated from mouse tail tips served as the template for qRT-PCRs. Different amounts of DNA from a WT mouse (containing two endogenous *Slc6a3* copies) were used to generate a standard curve and correlated with the respective C_t values. Analyses were carried out with Taqman Universal

PCR Master Mix (Life Technologies, #4304437) and a Taqman *Slc6a3* copy number assay (FAM) (Life Technologies, Mm00401145_cn).

Western blotting

Protein samples were obtained from the midbrain or striatum of three-to-four-month-old mice or from transfected HEK 293T cells. Cells were purchased from ATCC directly before use. Therefore, we did not carry out any authentication tests or tests for mycoplasma contamination. HEK 293T cells were chosen due to their high efficiency of transfection and protein production. Tissue samples were homogenized and protein concentrations determined using a BCA assay (Thermo Scientific). Equal amounts of protein were denatured in Laemmli buffer at 95°C for 5 min and separated using one of the following gels: 8-16% Tris-HCl (Biorad, #345-0038) (Supplementary Fig. 3d), 4-20% Tris-Glycine (Life Technologies, #EC6025) (SATB1 analysis), 10% Tris-Glycine (Life Technologies, #EC6075) (ZDHHC2 analysis). After transfer of proteins to nitrocellulose membranes, blots were blocked in 5% non-fat milk for 2 h at room temperature and incubated with the respective primary antibody at 4°C overnight. Primary antibodies were as follows: rabbit polyclonal anti-TH antibody (Millipore, #AB152; 1:1,000), rabbit polyclonal anti-DAT antibody (Millipore, #AB2231; 1:1,000), rabbit polyclonal anti-GAPDH antibody (Abcam, #ab9485; 1:4,000), rabbit monoclonal anti-SATB1 antibody (Abcam, #ab92307; 1:50), rabbit polyclonal anti-ZDHHC2 antibody (Novus, #NBP2-13541; 1:250), mouse monoclonal anti-β-tubulin (Sigma, #T5201; 1:2,000), and mouse monoclonal anti-FLAG M2 antibody (Sigma, #F1804; 1:4,000). Primary antibodies were detected using either HRP-linked donkey anti-rabbit IgG (GE Healthcare, #NA934V; 1:10,000) or HRP-linked sheep anti-mouse IgG (GE Healthcare, #NA931V, 1:10000 dilution) together with Western Lightning Plus-ECL (Perkin Elmer, #NEL105001EA). Bands were quantified with ImageJ software and normalized to the corresponding GAPDH or β-tubulin bands.

Viruses

All viruses were obtained from Vector Biolabs. AAV1-EGFP-U6-shRNA was used as the control (expression of scrambled shRNA and EGFP, #7040). Viruses for the silencing of *Satb1* or *Zdhhc2* were custom-made. For each target, 10 different shRNAs were validated in a HEK293 cell-based luciferase assay *in vitro* (Vector Biolabs) (Supplementary Tables 8, 9). The two shRNAs with the highest knockdown efficiency for *Satb1* and *Zdhhc2*, respectively, were selected for the generation of constructs for the *in vivo* experiments. *Satb1* shRNA constructs were designed to target bp 2329-2349 of *Satb1* mRNA or bp 2441-2461 of *Satb1* mRNA (shRNA #2) (reference sequence: BC011132.1) and included the coding sequence for EGFP or red fluorescent protein (RFP) (shRNA #2). *Zdhhc2* shRNA constructs were designed to target bp 720-740 of *Zdhhc2* mRNA or bp 373-393 of *Zdhhc2* mRNA (shRNA #2) (reference sequence: BC117761.1) and included the coding sequence for RFP or EGFP (shRNA #2). All four shRNA constructs were packaged into the same AAV1 virus that was used for the control vector. All viruses were injected at a concentration of 1×10^{13} GC/ml.

Stereotaxic surgery

All stereotaxic injections were carried out on an Angle Two stereotaxic frame for mouse with motorized nanoinjector (Leica). 10-week-old male C57BL/6 WT mice (Charles River Laboratories) were anesthetized with ketamine/xylazine and stereotaxically injected with AAV1-*Satb1* shRNA or AAV1-*Zdhhc2* shRNA into the ipsilateral SNpc (AP: -3.0 mm; ML: -1.2 mm; DV: -4.3 mm) or with AAV1-scrambled shRNA into the contralateral SNpc (AP: -3.0 mm; ML: +1.2 mm; DV: -4.3 mm). A subset of 10-week-old WT mice were stereotaxically injected with Fluorogold (Fluorochrome) in saline into the ipsilateral (AP: +0.9 mm; ML: -2.0 mm; DV: -3.2 mm) and contralateral (AP: +0.9 mm; ML: +2.0 mm; DV: -3.2 mm) dorsal striatum seven days prior to the stereotaxic injection of the viruses into the ipsilateral and contralateral SNpc. The total injection volume was 0.5 µl (viruses) or 0.25 µl (2% Fluorogold). All injections were performed at a rate of 0.05 µl/min using Hamilton syringes (30 gauge). Wounds were sutured and healing and recovery were monitored after the injections.

Histology

Three-to-four-month-old mice were anesthetized with pentobarbital and transcardially perfused using 1 × PBS, pH 7.4, followed by 4 % paraformaldehyde in 1 × PBS. Brains were removed from the skull, post-fixed for 1 h in 4 % paraformaldehyde in 1 × PBS at room temperature, cryopreserved using a gradient of 5 %, 15 % and 30 % sucrose, embedded in Neg-50 (Thermo Scientific), frozen and stored at -80 °C. Subsequently, using a Microm cryostat, 12-µm-thick sagittal or coronal sections were prepared, thaw mounted onto Superfrost Plus microscope slides (Fisher Scientific) and stored at -80 °C until immunostaining.

For EGFP immunohistochemistry (IHC) in combination with indirect immunofluorescence (IF) staining for TH, brain sections were washed in 1 × PBS, incubated in 0.2 % H_2O_2 in 1 × PBS, washed in 1 × PBS, permeabilized with 0.05 % Tween-20 in 1 × PBS, washed in 1 × PBS, blocked with Image-It FX signal enhancer (Life Technologies), washed with 0.05% Tween-20 in 1 × PBS, followed by blocking with 2 % donkey serum and 0.1 % fish gelatin in 0.05 % Tween-20 in 1 × PBS. Sections were then incubated with a rabbit polyclonal anti-EGFP antibody (Abcam, #ab6556) at a concentration of 1:5,000 and a mouse monoclonal anti-TH antibody (Sigma, #T2928) at a concentration of 1:250 at 4 °C overnight. The next day, slides were washed with 0.05% Tween-20 in 1 × PBS and incubated with Alexa Fluor 568 donkey anti-mouse IgG (Life Technologies, #A10037) at a concentration of 1:250 for 1 h. After another washing step, SuperPicture HRP Polymer Conjugate Rabbit Primary (Life Technologies, #87-9263) was applied for 1 h, followed by another washing step and incubation with Tyramide-Alexa Fluor 488 conjugate (Life Technologies, #T-20922) for 10 min. Subsequently, slides were washed, mounted with ProLong Gold Antifade (Life Technologies, #P36930), coverslipped and stored in the dark at room temperature until imaging.

ZDHHC2 IHC in combination with indirect IF staining for TH was carried out as described above, but 0.05 % Tween-20 was replaced by 0.2 % Triton X-100 in all steps on day one. The primary antibodies were a rabbit polyclonal anti-ZDHHC2 antibody (Novus

Biologicals, #NBP2-13541) used at a concentration of 1:500 and a chicken polyclonal anti-TH antibody (Millipore, #AB9702) used at a concentration of 1:250. On day two, all washing steps were carried out with 1 × PBS. For secondary detection, Alexa Fluor 546 goat anti-chicken IgG (Life Technologies, #A11040) was used at a concentration of 1:250 and SuperPicture HRP Polymer Conjugate Rabbit Primary (Life Technologies, #87-9263) was used together with Tyramide-Alexa Fluor 488 conjugate (Life Technologies, #T-20922) as described above. To visualize the Golgi apparatus, mouse monoclonal anti-GM130 antibody (BD Biosciences, #610822) was added at a concentration of 1:50 on day one and Alexa Fluor 633 goat anti-mouse IgG (Life Technologies, #A21052) was added at a concentration of 1:250 on day two. On tissue sections from stereotaxically injected mice, ZDHHC2 IHC in combination with indirect IF staining for TH was carried out as described above, using the following modifications: the primary rabbit polyclonal anti-ZDHHC2 antibody was used at a concentration of 1:50; a mouse monoclonal anti-TH antibody (Sigma, #T2928) was used at a concentration of 1:200; an Alexa Fluor 405 goat anti-mouse IgG (Life Technologies, #A31553) was used at a concentration of 1:200 and applied to the tissue sections for 2 h, SuperPicture HRP Polymer Conjugate Rabbit Primary (Life Technologies, #87-9263) was applied to the tissue sections for 2h, and Tyramide-Alexa Fluor 647 conjugate (Life Technologies, #T-20926) was applied for 15 min.

For indirect IF staining for TH or for TH in combination with SATB1, brain sections were washed in 1 × PBS, permeabilized with 0.2 % Triton X in 1 × PBS, followed by blocking with 2 % donkey serum and 0.1 % fish gelatin in 0.2 % Triton X in 1 × PBS. Sections were then incubated with one or several of the following primary antibodies at 4 °C overnight: rabbit polyclonal anti-TH antibody (Millipore, #AB152) at a concentration of 1:250, mouse monoclonal anti-TH antibody (Sigma, #T2928) at a concentration of 1:250, goat polyclonal anti-SATB1 antibody (Santa Cruz Biotechnology, #sc-5989) at a concentration of 1:100. The next day, slides were washed with 1 × PBS and incubated with one or several of the following secondary antibodies at a concentration of 1:250 for 1 h: Alexa Fluor 546 donkey anti-rabbit IgG (Life Technologies, #A10040), Alexa Fluor 488 donkey anti-goat IgG (Life Technologies, #A11055), Alexa Fluor 546 rabbit anti-mouse IgG (Life Technologies, #A11060), Alexa Fluor 546 donkey anti-goat IgG (Life Technologies, #A11056), Alexa Fluor 633 rabbit anti-mouse IgG (Life Technologies, #A21063). After another washing step, slides were mounted with ProLong Gold Antifade (Life Technologies, #P36930) or ProLong Gold Antifade with DAPI (Life Technologies, #P36931), coverslipped and stored at room temperature in the dark until imaging.

For hematoxylin and eosin staining, mice were euthanized with CO_2 and immediately necropsied. Tissues were fixed in 10 % neutral buffered formalin. Heads were decalcified using Surgipath Decalcifier I (Leica Microsystems, #3800400) and subsequently sectioned every 3-4 mm to yield 6-7 coronal sections. Tissue sections were processed through paraffin and then sectioned further and stained with hematoxylin and eosin. Fluorescent images were collected on a Zeiss LSM 710 confocal microscope. Images were minimally processed using Photoshop CS5 (Adobe Systems) to enhance brightness and contrast for optimal representation of the data. All histology findings were confirmed in at least three different animals.

Behavioral analyses

All behavioral analyses were carried out during the light cycle. The different tests were administered to the same group of animals. Rotarod testing was carried out on an apparatus from Med-Associates using a rod that accelerated at increasing speed from 4-40 rpm over 5 min. Mice completed one training trial, followed by three test trials per day for three consecutive days. Results from the three test trials were averaged. The body weights of TG Dat bacTRAP mice and WT littermates were significantly different at all ages (Supplementary Fig. 1b), and previous studies have demonstrated a negative correlation between body weight and rotarod performance [58,59]. Analysis of our data also revealed a significant correlation between body weight and rotarod performance for all mouse ages analyzed and on all test days ($P<0.05$). Therefore, rotarod results for each day were analyzed using One-Way ANCOVA for two independent samples, with body weight as a covariate (GraphPad Prism and http://vassarstats.net/ancova2L.html). For the pole test, a stand with an aluminum foil-wrapped pole that measured 19 inches in height and 1.25 inches in circumference was used. A training trial was administered to the mice the day before the experiment. The next day, mice completed five test trials. Results from the test trials were averaged. The wire hang test was carried out with a wire top from a mouse cage and included one training trial, followed by three test trials on the same day. Results from the three test trials were averaged. For the gait analysis, a 19-inches-long runway was used, together with a light source by the starting point and a dark box by the finish line. Mice underwent two to three test trials, and the most representative trace was selected for analysis. Food and water consumption were determined on single-housed mice for a period of 66-72 h. Food intake was measured by calculating the weight difference between the amounts of rodent diet in the mouse cage at the beginning and at the end of the observation period. Water intake was measured by calculating the volumetric difference between the water amounts in the bottles at the beginning and at the end of the observation period.

Assessment of key parameters of body composition

Total body water, extracellular and intracellular fluid, fat-free mass and fat mass of 12-month-old mice were determined using the ImpediVET equipment (ImpediMed) following the manufacturer's instructions.

Statistics

All experiments included three or more biological replicates. No statistical methods were used to pre-determine sample sizes but our sample sizes are similar to those generally employed in the field. Sample sizes are indicated by n-values in each figure legend. We excluded animals from data analysis if they were flagged by the Rockefeller University or Columbia University veterinary services for health reasons during the experimental period. Unless indicated otherwise in the respective methods section and/or figure legend, paired or unpaired one-tailed or two-tailed *t*-tests were applied for the comparison of two samples using GraphPad Prism. Paired testing was only applied to the comparison of data obtained from the same animal or the same group of animals. One-tailed testing was only applied to the analysis of TH^+ neurons after MR knockdown. Normality and equality of variance were formally tested using GraphPad Prism. All data represent means ± SEM. Prior to data

collection, outliers were defined as data points located outside the range of mean±2*SD. No specific method of randomization was used to assign animals to experimental groups. Investigators were not blinded to the group allocation.

Supplementary Material

Refer to Web version on PubMed Central for supplementary material.

Acknowledgments

We are grateful to Nathaniel Heintz, Eric Schmidt and Myriam Heiman for consultations on TRAP analysis, to Mallory Kerner and Jason Ni for assistance with stereotaxic injections, to Begum Sezer, Gabriela Bustamante, Thomas Kassel and Kevin Dam for assistance with genotyping, qRT-PCR and behavioral experiments, to Jodi Gresack for consultations on behavioral experiments, to Elisabeth Griggs for assistance with the graphic design, and to Joseph Terlizzi for commenting on the manuscript. We thank Transgenic Services and the Genomics Core at Rockefeller University as well as the Tri-Institutional Laboratory of Comparative Pathology and the Molecular Cytogenetics Core at Memorial Sloan-Kettering Cancer Center for technical support. This study was supported by US Army Medical Research contracts W81XWH-10-1-0640 and W81XWH-12-1-0039 (to L.B.), by Parkinson's Disease Foundation Center Grant #CU51523608 and US Army Medical Research contracts W81XWH-08-1-0465 and W81XWH-10-1-053 (to S.P.), and by US Army Medical Research contract W81XWH-09-1-0402 and the JPB Foundation (to P.G.).

References

1. Heiman M, et al. A translational profiling approach for the molecular characterization of CNS cell types. Cell. 2008; 135:738–748. [PubMed: 19013281]
2. Doyle JP, et al. Application of a translational profiling approach for the comparative analysis of CNS cell types. Cell. 2008; 135:749–762. [PubMed: 19013282]
3. Sanz E, et al. Cell-type-specific isolation of ribosome-associated mRNA from complex tissues. Proc Natl Acad Sci U S A. 2009; 106:13939–13944. [PubMed: 19666516]
4. Kanehisa M. A database for post-genome analysis. Trends Genet. 1997; 13:375–376. [PubMed: 9287494]
5. Huang da W, Sherman BT, Lempicki RA. Systematic and integrative analysis of large gene lists using DAVID bioinformatics resources. Nature Protocols. 2009; 4:44–57. [PubMed: 19131956]
6. Huang da W, Sherman BT, Lempicki RA. Bioinformatics enrichment tools: paths toward the comprehensive functional analysis of large gene lists. Nucleic Acids Res. 2009; 37:1–13. [PubMed: 19033363]
7. Carter RJ, Morton J, Dunnett SB. Motor coordination and balance in rodents. Curr Protoc Neurosci. 2001; Chapter 8:12. Unit 8. [PubMed: 18428540]
8. Dauer W, Przedborski S. Parkinson's disease: mechanisms and models. Neuron. 2003; 39:889–909. [PubMed: 12971891]
9. Jackson-Lewis V, Przedborski S. Protocol for the MPTP mouse model of Parkinson's disease. Nature Protocols. 2007; 2:141–151. [PubMed: 17401348]
10. Jackson-Lewis V, Blesa J, Przedborski S. Animal models of Parkinson's disease. Parkinsonism Relat Disord. 2012; 18(Suppl 1):S183–185. [PubMed: 22166429]
11. Vila M, et al. Bax ablation prevents dopaminergic neurodegeneration in the 1-methyl- 4-phenyl-1,2,3,6-tetrahydropyridine mouse model of Parkinson's disease. Proc Natl Acad Sci U S A. 2001; 98:2837–2842. [PubMed: 11226327]
12. Damier P, Hirsch EC, Agid Y, Graybiel AM. The substantia nigra of the human brain. II Patterns of loss of dopamine-containing neurons in Parkinson's disease Brain. 1999; 122(Pt 8):1437–1448. [PubMed: 10430830]
13. Hirsch E, Graybiel AM, Agid YA. Melanized dopaminergic neurons are differentially susceptible to degeneration in Parkinson's disease. Nature. 1988; 334:345–348. [PubMed: 2899295]

14. Jackson-Lewis V, Jakowec M, Burke RE, Przedborski S. Time course and morphology of dopaminergic neuronal death caused by the neurotoxin 1-methyl-4-phenyl-1,2,3,6-tetrahydropyridine. Neurodegeneration. 1995; 4:257–269. [PubMed: 8581558]
15. Muthane U, et al. Differences in nigral neuron number and sensitivity to 1-methyl-4-phenyl-1,2,3,6-tetrahydropyridine in C57/bl and CD-1 mice. Exp Neurol. 1994; 126:195–204. [PubMed: 7925820]
16. Bowenkamp KE, et al. 6-hydroxydopamine induces the loss of the dopaminergic phenotype in substantia nigra neurons of the rat. A possible mechanism for restoration of the nigrostriatal circuit mediated by glial cell line-derived neurotrophic factor. Exp Brain Res. 1996; 111:1–7. [PubMed: 8891630]
17. Piovan E, et al. Direct reversal of glucocorticoid resistance by AKT inhibition in acute lymphoblastic leukemia. Cancer Cell. 2013; 24:766–776. [PubMed: 24291004]
18. Lefebvre C, et al. A human B-cell interactome identifies MYB and FOXM1 as master regulators of proliferation in germinal centers. Mol Syst Biol. 2010; 6:377. [PubMed: 20531406]
19. Carro MS, et al. The transcriptional network for mesenchymal transformation of brain tumours. Nature. 2010; 463:318–325. [PubMed: 20032975]
20. Aytes A, et al. Cross-species regulatory network analysis identifies a synergistic interaction between FOXM1 and CENPF that drives prostate cancer malignancy. Cancer Cell. 2014; 25:638–651. [PubMed: 24823640]
21. Margolin AA, et al. ARACNE: an algorithm for the reconstruction of gene regulatory networks in a mammalian cellular context. BMC Bioinformatics. 2006; 7(Suppl 1):S7. [PubMed: 16723010]
22. Chen JC, et al. Identification of causal genetic drivers of human disease through systems-level analysis of regulatory networks. Cell. 2014; 159:402–414. [PubMed: 25303533]
23. Repunte-Canonigo V, et al. Identifying candidate drivers of alcohol dependence-induced excessive drinking by assembly and interrogation of brain-specific regulatory networks. Genome Biol. 2015; 16:68. [PubMed: 25886852]
24. Aubry S, et al. Assembly and interrogation of Alzheimer's disease genetic networks reveal novel regulators of progression. PloS One. 2015; 10:e0120352. [PubMed: 25781952]
25. Chung CY, et al. Cell type-specific gene expression of midbrain dopaminergic neurons reveals molecules involved in their vulnerability and protection. Hum Mol Genet. 2005; 14:1709–1725. [PubMed: 15888489]
26. Huang Y, et al. Distribution of Satb1 in the central nervous system of adult mice. Neurosci Res. 2011; 71:12–21. [PubMed: 21658419]
27. Close J, et al. Satb1 is an activity-modulated transcription factor required for the terminal differentiation and connectivity of medial ganglionic eminence-derived cortical interneurons. J Neurosci. 2012; 32:17690–17705. [PubMed: 23223290]
28. Zheng B, et al. PGC-1alpha, a potential therapeutic target for early intervention in Parkinson's disease. Sci Transl Med. 2010; 2 52ra73.
29. Grimm J, Mueller A, Hefti F, Rosenthal A. Molecular basis for catecholaminergic neuron diversity. Proc Natl Acad Sci U S A. 2004; 101:13891–13896. [PubMed: 15353588]
30. Greene JG, Dingledine R, Greenamyre JT. Gene expression profiling of rat midbrain dopamine neurons: implications for selective vulnerability in parkinsonism. Neurobiol Dis. 2005; 18:19–31. [PubMed: 15649693]
31. Phani S, Gonye G, Iacovitti L. VTA neurons show a potentially protective transcriptional response to MPTP. Brain Res. 2010; 1343
32. Greene JG, Dingledine R, Greenamyre JT. Neuron-selective changes in RNA transcripts related to energy metabolism in toxic models of parkinsonism in rodents. Neurobiol Dis. 2010; 38:476–481. [PubMed: 20307667]
33. Miller RM, et al. Wild-type and mutant alpha-synuclein induce a multi-component gene expression profile consistent with shared pathophysiology in different transgenic mouse models of PD. Exp Neurol. 2007; 204:421–432. [PubMed: 17254569]
34. Bifsha P, Yang J, Fisher RA, Drouin J. Rgs6 is Required for Adult Maintenance of Dopaminergic Neurons in the Ventral Substantia Nigra. PLoS Genetics. 2014; 10:e1004863. [PubMed: 25501001]

35. Ryan SD, et al. Isogenic human iPSC Parkinson's model shows nitrosative stress-induced dysfunction in MEF2-PGC1alpha transcription. Cell. 2013; 155:1351–1364. [PubMed: 24290359]
36. Okamoto S, Krainc D, Sherman K, Lipton SA. Antiapoptotic role of the p38 mitogen-activated protein kinase-myocyte enhancer factor 2 transcription factor pathway during neuronal differentiation. Proc Natl Acad Sci U S A. 2000; 97:7561–7566. [PubMed: 10852968]
37. Cho EG, et al. MEF2C enhances dopaminergic neuron differentiation of human embryonic stem cells in a parkinsonian rat model. PloS One. 2011; 6:e24027. [PubMed: 21901155]
38. Gantz SC, Ford CP, Neve KA, Williams JT. Loss of Mecp2 in substantia nigra dopamine neurons compromises the nigrostriatal pathway. J Neurosci. 2011; 31:12629–12637. [PubMed: 21880923]
39. Panayotis N, et al. Morphological and functional alterations in the substantia nigra pars compacta of the Mecp2-null mouse. Neurobiol Dis. 2011; 41:385–397. [PubMed: 20951208]
40. Chan CS, et al. 'Rejuvenation' protects neurons in mouse models of Parkinson's disease. Nature. 2007; 447:1081–1086. [PubMed: 17558391]
41. Guzman JN, et al. Oxidant stress evoked by pacemaking in dopaminergic neurons is attenuated by DJ-1. Nature. 2010; 468:696–700. [PubMed: 21068725]
42. Mosharov EV, et al. Interplay between cytosolic dopamine, calcium, and alpha-synuclein causes selective death of substantia nigra neurons. Neuron. 2009; 62:218–229. [PubMed: 19409267]
43. Yasui D, Miyano M, Cai S, Varga-Weisz P, Kohwi-Shigematsu T. SATB1 targets chromatin remodelling to regulate genes over long distances. Nature. 2002; 419:641–645. [PubMed: 12374985]
44. Roth AF, et al. Global analysis of protein palmitoylation in yeast. Cell. 2006; 125:1003–1013. [PubMed: 16751107]
45. Kostiuk MA, Keller BO, Berthiaume LG. Palmitoylation of ketogenic enzyme HMGCS2 enhances its interaction with PPARalpha and transcription at the Hmgcs2 PPRE. FASEB J. 2010; 24:1914–1924. [PubMed: 20124434]
46. Wang K, et al. Genome-wide identification of post-translational modulators of transcription factor activity in human B cells. Nat Biotechnol. 2009; 27:829–839. [PubMed: 19741643]
47. Gong S, et al. A gene expression atlas of the central nervous system based on bacterial artificial chromosomes. Nature. 2003; 425:917–925. [PubMed: 14586460]
48. Heiman M, Kulicke R, Fenster RJ, Greengard P, Heintz N. Cell type-specific mRNA purification by translating ribosome affinity purification (TRAP). Nature Protocols. 2014; 9:1282–1291. [PubMed: 24810037]
49. Langmead B, Trapnell C, Pop M, Salzberg SL. Ultrafast and memory-efficient alignment of short DNA sequences to the human genome. Genome Biol. 2009; 10:R25. [PubMed: 19261174]
50. Gentleman RC, et al. Bioconductor: open software development for computational biology and bioinformatics. Genome Biol. 2004; 5:R80. [PubMed: 15461798]
51. Trapnell C, Pachter L, Salzberg SL. TopHat: discovering splice junctions with RNA-Seq. Bioinformatics. 2009; 25:1105–1111. [PubMed: 19289445]
52. Trapnell C, et al. Transcript assembly and quantification by RNA-Seq reveals unannotated transcripts and isoform switching during cell differentiation. Nat Biotechnol. 2010; 28:511–515. [PubMed: 20436464]
53. Anders S, Huber W. Differential expression analysis for sequence count data. Genome Biol. 2010; 11:R106. [PubMed: 20979621]
54. Liberatore GT, et al. Inducible nitric oxide synthase stimulates dopaminergic neurodegeneration in the MPTP model of Parkinson disease. Nat Med. 1999; 5:1403–1409. [PubMed: 10581083]
55. Przedborski S, et al. Role of neuronal nitric oxide in 1-methyl-4-phenyl-1,2,3,6-tetrahydropyridine (MPTP)-induced dopaminergic neurotoxicity. Proc Natl Acad Sci U S A. 1996; 93:4565–4571. [PubMed: 8643444]
56. Ashburner M, et al. Gene ontology: tool for the unification of biology. The Gene Ontology Consortium Nat Genet. 2000; 25:25–29. [PubMed: 10802651]
57. Subramanian A, et al. Gene set enrichment analysis: a knowledge-based approach for interpreting genome-wide expression profiles. Proc Natl Acad Sci U S A. 2005; 102:15545–15550. [PubMed: 16199517]

58. Brown RE, Wong AA. The influence of visual ability on learning and memory performance in 13 strains of mice. Learn Mem. 2007; 14:134–144. [PubMed: 17351136]

59. McFadyen MP, Kusek G, Bolivar VJ, Flaherty L. Differences among eight inbred strains of mice in motor ability and motor learning on a rotorod. Genes Brain Behav. 2003; 2:214–219. [PubMed: 12953787]

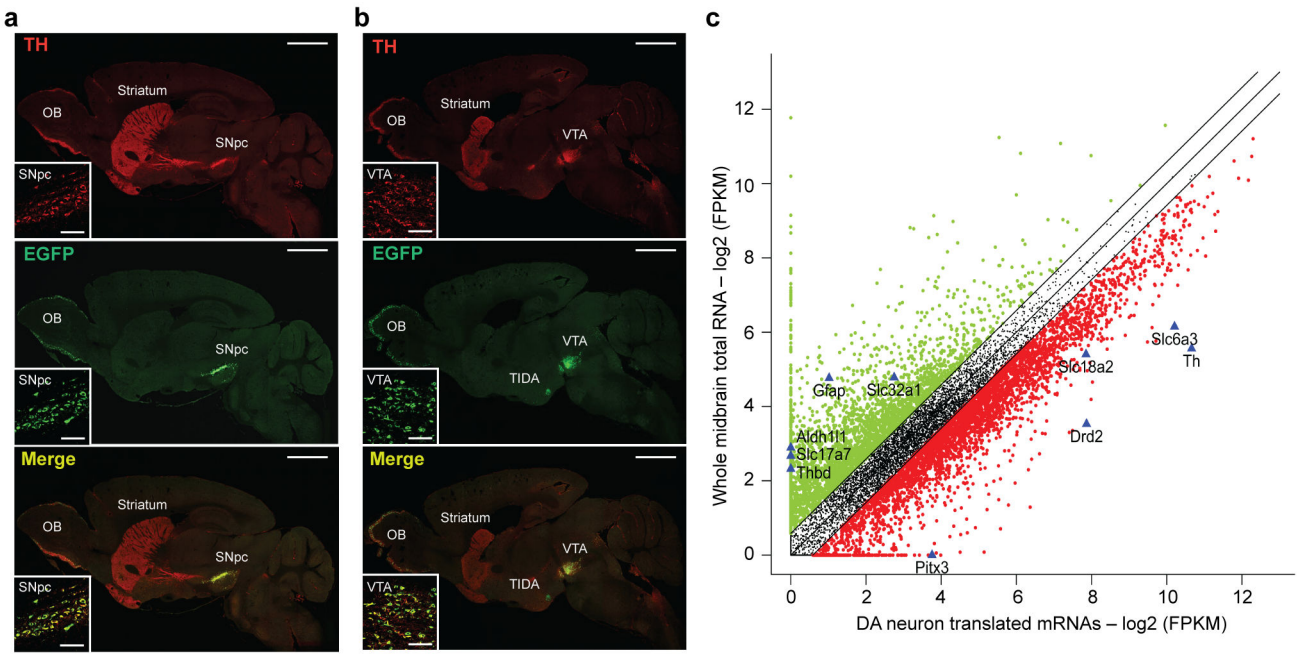

Figure 1. Generation of Dat bacTRAP mice for the translational profiling of midbrain DA neurons

(a) Sagittal brain section from a Dat bacTRAP mouse stained for TH (red) and EGFP (green) at the level of the SNpc. (b) Sagittal brain section from a Dat bacTRAP mouse stained for TH (red) and EGFP (green) at the level of the VTA. (c) Mean gene expression values obtained from whole midbrain total RNA samples (n=5) plotted against mean gene expression values from midbrain DA neuron TRAP samples (n=4). Lines to each side represent 1.5fold enrichment in either sample. The center line represents equal expression. Red dots represent transcripts enriched in the DA neuron TRAP samples by ≥1.5fold (P<0.05). Green dots represent transcripts enriched in whole midbrain total RNA samples by ≥1.5fold (P<0.05). Black dots represent non-significant transcripts. Blue triangles depict select marker genes. *Scale bars, 2 mm in (a) and (b) (main images) and 60 μm in (a) and (b) (inserts). n-values indicate biological replicates.*

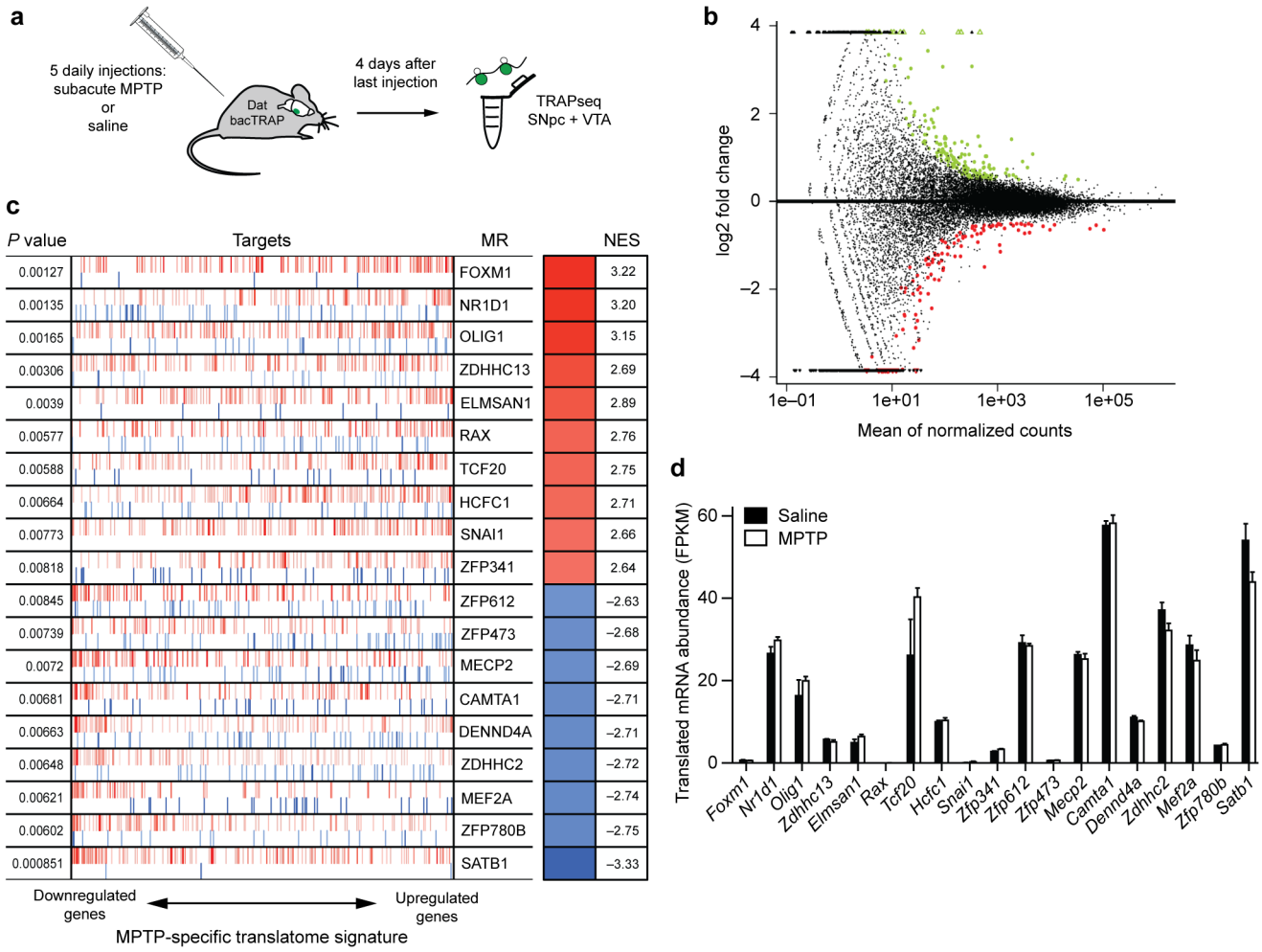

Figure 2. TRAPseq analysis in a mouse model of PD and regulatory network analysis

(a) Time line for TRAPseq analysis of midbrain DA neurons after injection of Dat bacTRAP mice with MPTP (n=4) or saline (vehicle; n=4).(b) Comparative analysis of the translatome libraries obtained from unperturbed midbrain DA neurons in saline-treated Dat bacTRAP mice (n=4) or from DA neurons under toxin-induced stress in MPTP-treated Dat bacTRAP mice (n=4). Log2 fold change values were plotted against mean gene expression values. The center line represents equal expression. Green dots represent transcripts with a ≥1.5fold increased expression in MPTP-treated samples (P<0.05). Red dots represent transcripts with a ≥1.5fold decreased expression in MPTP-treated samples (P<0.05). Black dots represent non-significant transcripts. (c) Statistically significant MRs (P<0.01) determined by MARINa analysis for the MPTP-specific translatome signature obtained in panel (a). Each row of the plot shows the MARINa results obtained for the respective MR. The heatmap on the right shows the predicted MR activity, with red indicating an increase of activity in MPTP-treated samples [corresponding to a positive Normalized Enrichment Score (NES)], and blue indicating a decrease (corresponding to a negative NES). NES values were calculated by MARINa. The x-axis represents the MPTP-specific translatome signature, arranged from the gene with the greatest decrease in expression to the gene with the greatest

increase in expression, compared to control. The vertical red and blue lines correspond to ARACNe-predicted target genes of the respective MR. Positively regulated target genes (expression induced by the MR) are shown in red. Negatively regulated target genes (expression repressed by the MR) are shown in blue. Increased activity of an MR is indicated by the significant enrichment of its positive targets among the up-regulated genes in the MPTP translatome signature, and its negative targets among the down-regulated genes in the MPTP translatome signature. Conversely, decreased MR activity is indicated by the significant enrichment of its positive targets among the down-regulated genes in the MPTP translatome signature, and its negative targets among the up-regulated genes in the MPTP translatome signature. Identity and differential expression values of the ARACNe-predicted targets for each displayed MR are provided in Supplementary Table 4. (d) MR expression levels in TRAPseq samples obtained in panel (a). P=0.647 (*Foxm1*); P=0.125 (*Nr1d1*); P=0.397 (*Olig1*); P=0.272 (*Zdhhc13*); P=0.189 (*Elmsan1*); P=0.237 (*Rax*); P=0.168 (*Tcf20*); P=0.665 (*Hcfc1*); P=0.139 (*Snai1*); P=0.053 (*Zfp341*); P=0.707 (*Zfp612*); P=0.367 (*Zfp473*); P=0.501 (*Mecp2*); P=0.802 (*Camta1*); P=0.114 (*Dennd4a*); P=0.103 (*Zdhhc2*); P=0.321 (*Mef2a*); P=0.512 (*Zfp780b*); P=0.080 (*Satb1*). Unpaired t-test. FPKM, fragments per kilobase per million. *n-values indicate biological replicates. Data in (d) represent means ± SEM.*

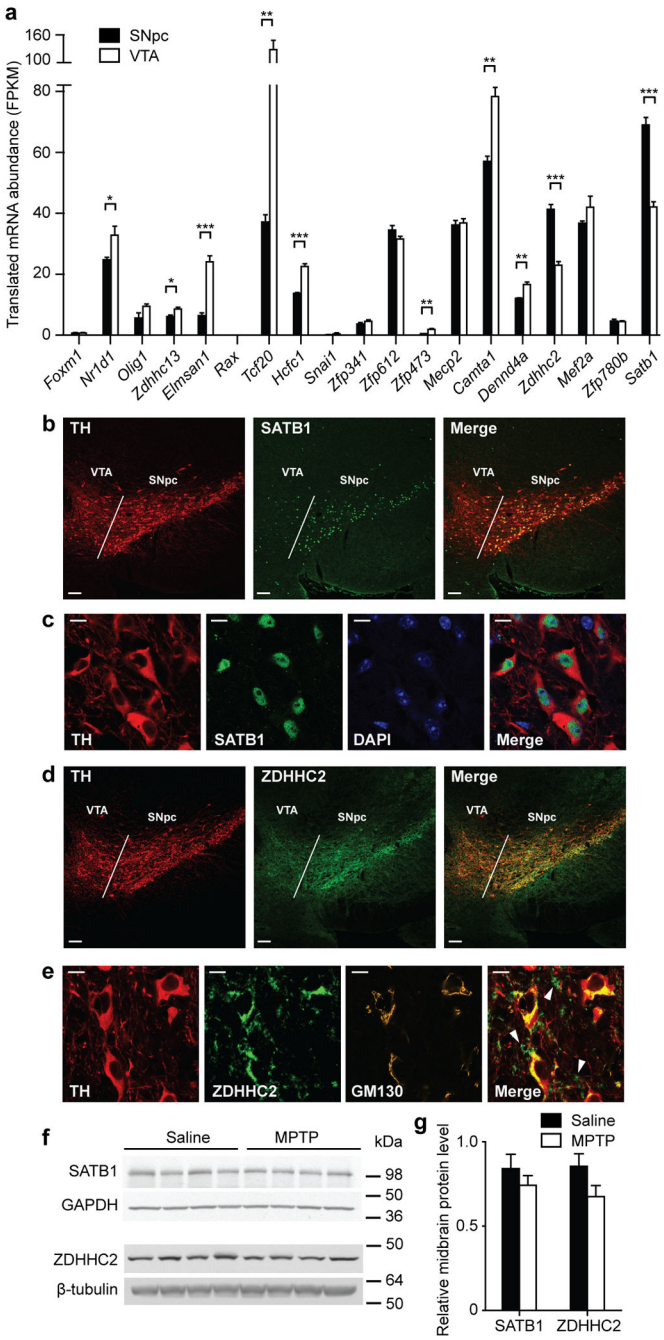

Figure 3. Analysis of MR expression patterns in midbrain DA neurons

(a) MR expression levels in TRAPseq samples from either SNpc or VTA DA neurons obtained from Dat bacTRAP mice (n=6). *P*=0.862 (*Foxm1*); *P*=0.042 (*Nr1d1*); *P*=0.094 (*Olig1*); *P*=0.014 (*Zdhhc13*); *P*=0.0001 (*Elmsan1*); *P*=0.740 (*Rax*); *P*=0.005 (*Tcf20*); *P*=0.0004 (*Hcfc1*); *P*=0.317 (*Snai1*); *P*=0.214 (*Zfp341*); *P*=0.210 (*Zfp612*); *P*=0.002 (*Zfp473*); *P*=0.754 (*Mecp2*); *P*=0.003 (*Camta1*); *P*=0.001 (*Dennd4a*); *P*=0.0001 (*Zdhhc2*); *P*=0.186 (*Mef2a*); *P*=0.733 (*Zfp780b*); *P*=0.0001 (*Satb1*). Paired t-test. FPKM, fragments per kilobase per million. (b) Coronal brain sections from WT mice stained for TH (red) and

SATB1 (green). White lines indicate the border between SNpc and VTA. (c) SNpc DA neurons in WT mice stained for TH (red) and SATB1 (green) with DAPI counterstain (blue). (d) Coronal brain sections from WT mice stained for TH (red) and ZDHHC2 (green). White lines indicate the border between SNpc and VTA. (e) SNpc DA neurons in WT mice stained for TH (red), ZDHHC2 (green) and the Golgi marker GM130 (orange). White arrow heads indicate signal for ZDHHC2 that does not co-localize with that for TH. (f, g), Quantification of SATB1 and ZDHHC2 protein levels in midbrain from WT mice injected with either saline (n=4) or MPTP (n=4) according to Fig. 2a. GAPDH and β-tubulin, respectively, were used as loading controls. The molecular weight standard is shown on the right of the blot. SATB1: P=0.374; ZDHHC2: P=0.118. Unpaired t-test. Blot images are cropped. Full-length blots are presented in Supplementary Figure 9f-i. *n-values indicate biological replicates. Data in (a) and (g) represent means ± SEM. Scale bars, 100 μm in (b) and (d) and 10 μm in (c) and (e).* *P<0.05, **P<0.01, ***P<0.001.

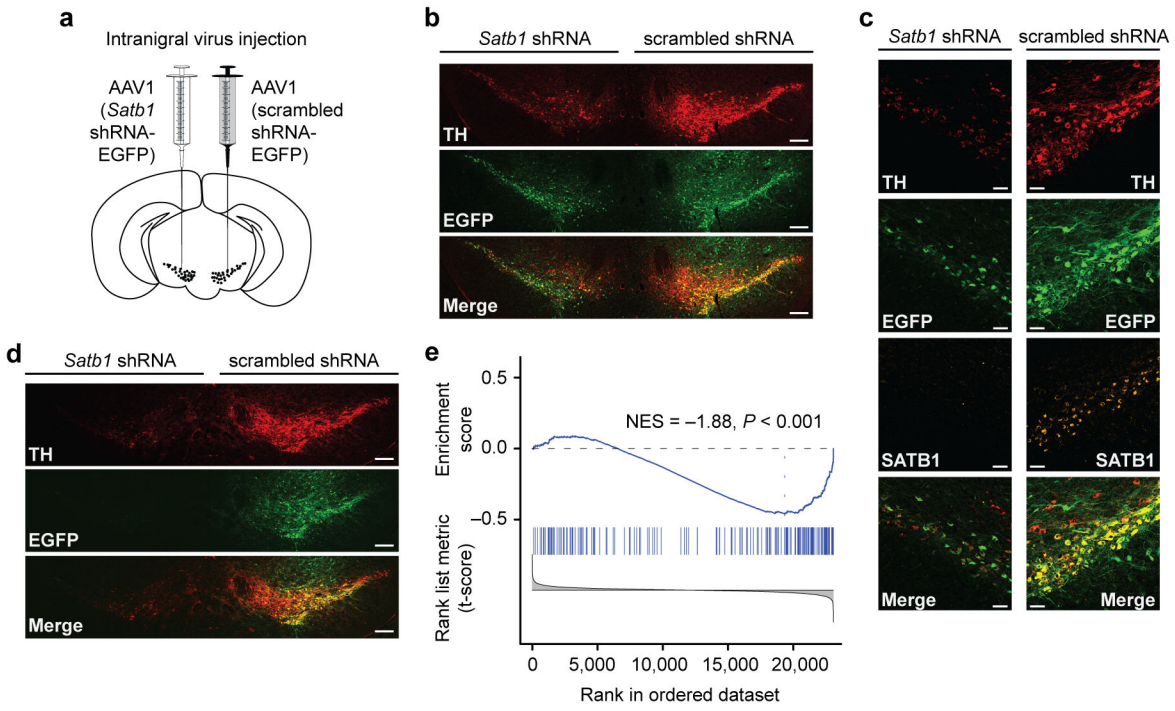

Figure 4. Virus-mediated knockdown of SATB1 in SNpc DA neurons

(a) Schematic illustration of bilateral stereotaxic AAV1 injections into the SNpc of WT mice using a *Satb1* shRNA-EGFP construct (ipsilateral side) or a scrambled shRNA-EGFP construct (contralateral side; control). (b) Coronal brain section from WT mice two weeks post-injection according to panel (a) showing staining for TH (red) and EGFP autofluorescence (green). (c) Coronal brain section from WT mice two weeks post-injection according to panel (a) showing staining for TH (red) and SATB1 (orange) as well as EGFP autofluorescence (green). (d) Coronal brain section from WT mice three weeks post-injection according to panel (a) showing staining for TH (red) and EGFP autofluorescence (green). (e) GSEA of SATB1 target genes (vertical bars) on a ranked list of genes differentially expressed after *Satb1* silencing in Dat bacTRAP mice according to (a) (n=3), sorted by their t-statistics. Genes that are downregulated after *Satb1* silencing received high rank numbers and are displayed in the right part of the plot. The blue line in the upper part of the plot indicates the GSEA enrichment running score. *Scale bars, 200 μm in (b) and (d) and 50 μm in (c). n-values indicate biological replicates.*

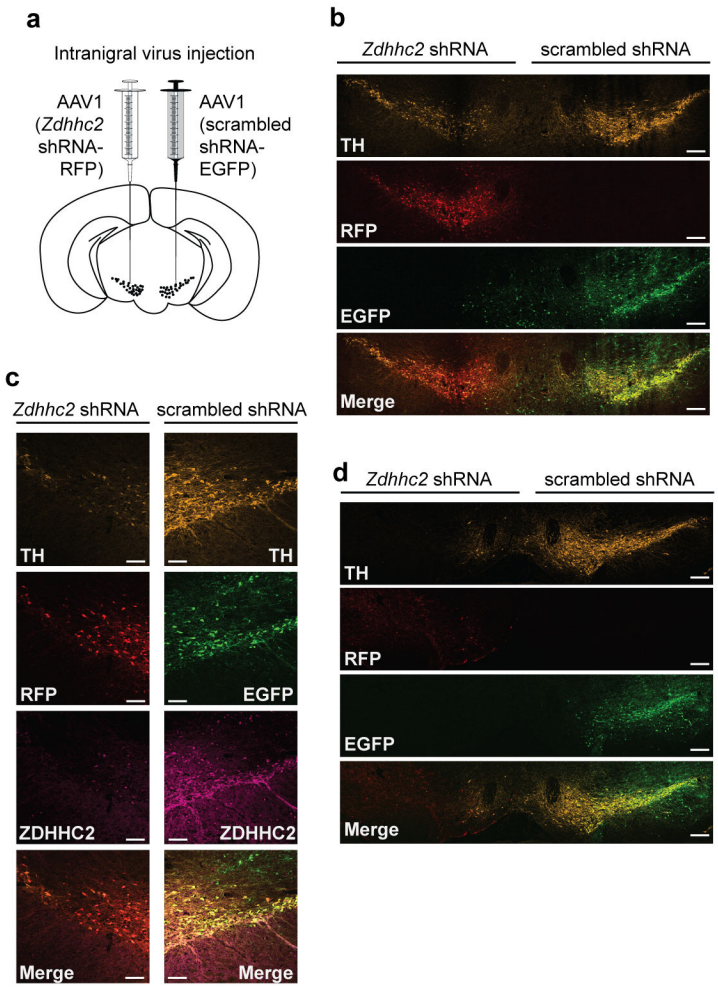

Figure 5. Virus-mediated knockdown of ZDHHC2 in SNpc DA neurons

(a) Schematic illustration of bilateral stereotaxic AAV1 injections into the SNpc of WT mice using a *Zdhhc2* shRNA-RFP construct (ipsilateral side) or a scrambled shRNA-EGFP construct (contralateral side; control). (b) Coronal brain section from WT mice one week post-injection according to panel (a) showing staining for TH (orange) as well as autofluorescence of RFP (red) and EGFP (green). (c) Coronal brain section from WT mice one week post-injection according to panel (a) showing staining for TH (orange) and ZDHHC2 (magenta) as well as autofluorescence of RFP (red) and EGFP (green). (d) Coronal brain section from WT mice two weeks post-injection according to panel (a) showing staining for TH (orange) as well as autofluorescence of RFP (red) and EGFP (green). *Scale bars, 200 μm in (b) and (d) and 100 μm in (c).*

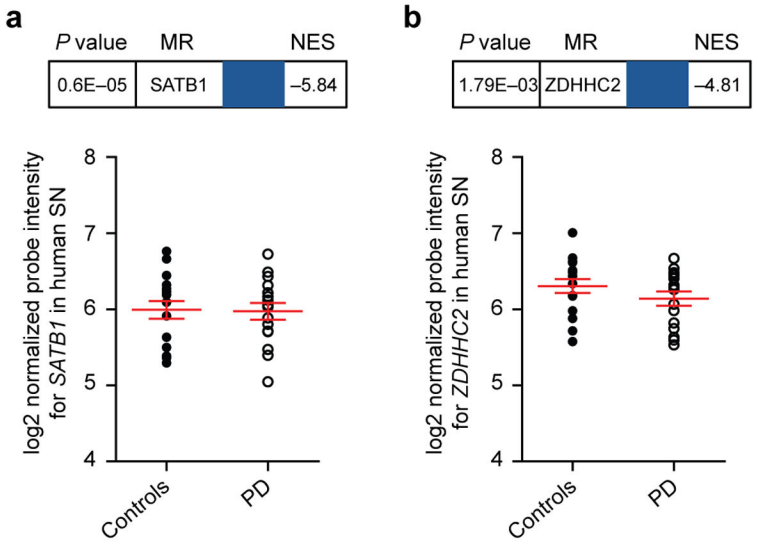

Figure 6. Master Regulator (MR) analysis on incipient PD expression signatures and controls

(a) Identification of SATB1 as a MR in SN samples from incipient PD cases (with blue indicating a decrease of activity; *P*=0.6E–5, MARINa analysis) and relative *SATB1* expression levels in SN from incipient PD cases (n=16) and controls (n=17). *P*=0.9069, unpaired t-test. (b) Identification of ZDHHC2 as a MR in SN samples from incipient PD cases (with blue indicating a decrease of activity; *P*=1.79E–3, MARINa analysis) and relative *ZDHHC2* expression levels in SN from incipient PD cases (n=16) and controls (n=17). *P*=0.2170, unpaired t-test. *n-values indicate biological replicates. Red lines and error bars indicate means ± SEM.*